Experimental robustness of the fractional topological phase to dephasing noise

R. A. Ribeiro,[1] A. A. Matoso,[1] L. E. Oxman,[2] A. Z. Khoury,[2] and S. Pádua[1,*]
[1]*Departamento de Física, Universidade Federal de Minas Gerais, 31270-901 Belo Horizonte, Minas Gerais, Brazil*
[2]*Instituto de Física, Universidade Federal Fluminense, 24210-346 Niterói, Rio de Janeiro, Brazil*

(Received 21 November 2021; accepted 26 October 2022; published 12 December 2022)

We observe experimentally the fractional topological phase (FTP) robustness to the dephasing noise in two-qudit photonic systems. We use a source of photon pairs generated by spontaneous parametric down-conversion, hyperentangled in the polarization and photon path degrees of freedom. The dephasing noise is described theoretically via Kraus maps and experimentally implemented via the spatial light modulator. The FTP is a great candidate to explore in the implementation of quantum processing and communication due to its robustness to dephasing noise.

DOI: 10.1103/PhysRevA.106.062411

The concept of geometric phase was introduced by Pancharatnam during a study of the light polarization transformation on the Poincaré sphere in classical optics [1]. Its quantum version, presented by Berry, was associated with the adiabatic evolution of a quantum state under the action of a time-dependent Hamiltonian [2]. Berry used the adiabatic theorem to deduce the geometric phase, but this restriction is not necessary for its manifestation, as pointed out by Aharonov and Anandan [3], who obtained the key result for the geometric phase γ_g,

$$\gamma_g = \arg\langle\psi(0)|\psi(t)\rangle + i\int_0^t dt'\,\langle\psi(t')|\dot{\psi}(t')\rangle\,, \qquad (1)$$

where $\psi(t)$ is the state vector at time t. The quantity given by Eq. (1) is invariant under any attempt of redefining the phase of the state vector along the time evolution, that is, γ_g is not sensitive to any transformation of the kind $|\psi(t)\rangle \rightarrow e^{i\varphi(t)}|\psi(t)\rangle$. This is the gauge invariance property of the geometric phase, which is behind its robustness against phase noise in quantum gate implementations [4].

In the years following Berry's studies, experimental works about the geometric phase [5–7] made use of the term *topological* for the phase dependence on the path traced in the state space. However, the connectedness of the corresponding spaces was not discussed. Kwiat and Chiao observed the geometric phase in bipartite states using a photonic system and two-photon interferometry, thus ensuring that it manifests in an optical system at the quantum level [8]. Hessmo and Sjöqvist's works [9,10] about the entanglement influence on geometric phase pointed to the existence of the topological phase. They showed that the geometric phase of the maximally entangled state of two qubits could have only two values, 0 or π. Milman and Mosseri proved that these two values originate from two distinct homotopy classes of closed paths traced in the manifold representing maximally entangled states of two qubits [11,12].

Sjöqvist reported a quantum kinematic method to describe the geometric phase for mixed states under nonunitary evolutions and discussed a way to measure the geometric phase for these states [13]. An experimental work by Du *et al.* [14] measured the geometric phase for a mixed state, whose results agree with the theoretical prediction [15]. This gives rise to the question whether an evolved mixed state can also acquire a topological phase and if it would be robust to noise.

Souza *et al.* [16] and Du *et al.* [17] experimentally observed the topological phase for two qubits. The generalization for two qudits came with the work by Oxman and Khoury [18], who showed that the topological phase appears in multiples of fractional values $2\pi/d$, where d is the individual dimension of the qudits. This phase is referred to as the fractional topological phase (FTP). Its topological nature originates in the multiple connectedness of the space formed by maximally entangled two-qudit states. Later the fractional values were also shown to occur in multiple-qubit systems [19,20]. The relationship between the fractional topological phase and entanglement in a two-qubit system was investigated in Ref. [21].

The experimental demonstration of the fractional phase values has been achieved with spatial qudits encoded in entangled photon pairs [22–24]. The theoretical investigation of the fractional topological phase robustness to dephasing noise was done in Refs. [25–31]. However, no experimental demonstration has been presented so far, which is a key requirement for practical applications in quantum phase gates. In this work we demonstrate experimentally the topological phase robustness against the action of a dephasing quantum channel.

The experimental setup is shown in Fig. 1. A 355-nm laser with vertical polarization becomes polarized at 45° after passing through a half waveplate (HWP) oriented at 22.5° with respect to the vertical direction. A controllable phase factor $e^{i\lambda}$ is introduced between the horizontal and vertical components when the beam crosses a quarter waveplate (QWP) oriented at 0°, slightly tilted around the horizontal axis perpendicular to the beam propagation direction. After crossing the lens L_p, the laser beam pumps two bismuth borate (BiBO) nonlinear

*Corresponding author: spadua@fisica.ufmg.br

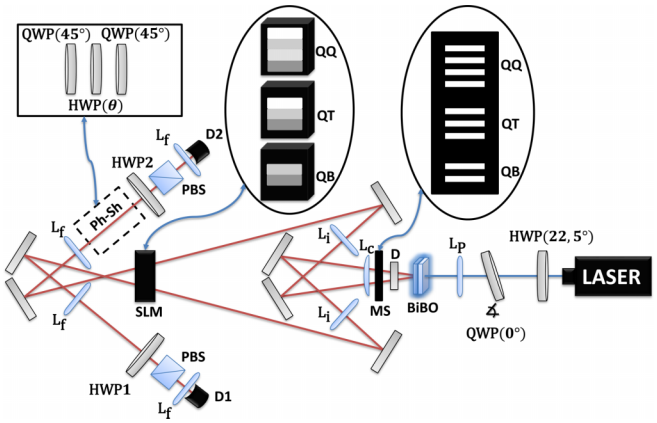

FIG. 1. Experimental setup (top view) for measuring the FTP in a two-qudit photonic system under dephasing noise: HWP, half waveplate; QWP, quarter waveplate; L_p, L_C, L_i, and L_f: lenses; D, dichroic mirror; MS, multiple slits; SLM, spatial light modulator; PBS, polarizing beam splitter; D1 and D2, avalanche photon detectors.

crystals cut for a type-I phase match. The crystals are glued together, with their optical axes orthogonal to each other. By spontaneous parametric down-conversion, they generate two noncollinear beams of photon pairs at 710 nm [32]. The two-photon state generated is entangled in the polarization degree of freedom [32] and can be written as $|\psi\rangle = \frac{1}{\sqrt{2}}(|H,H\rangle + e^{i\lambda}|V,V\rangle)$. By suitably tilting the QWP at the pump beam path, we set $e^{i\lambda} = -1$ [32]. A dichroic mirror reflects the pump beam and transmits the twin beams to an array of multiple slits positioned after the nonlinear crystals at the focal plane of the lens L_p. The slits are 100 μm wide, with a center-to-center separation of 250 μm. This arrangement generates an entangled state in the transverse path degree of freedom [33], where the number of slits sets the dimension of the qudits. Each transverse path selected by a certain slit is called a slit mode. Thus, taking into account both the polarization and the transverse path degrees of freedom, we have a source of photons in a hyperentangled state, which can be written as [24]

$$|\Psi\rangle = \frac{1}{\sqrt{2}}\alpha_{m,n}(|mH,nH\rangle - |mV,nV\rangle), \tag{2}$$

where $m,n = 1,\ldots,d$. For notation simplicity, we use the Einstein summation convention throughout the text. The superposition state between the two-qudit spatial state with the two photons with horizontal polarization or vertical polarization is a crucial ingredient of the setup. We measure the fractional topological phases through interference between the initial two-qudit state and the SU(d) transformed state. This requires controlled quantum operations, where the spatial degree of freedom is the target and the polarization is the control. We can rewrite it more compactly as $|\Psi\rangle = \alpha^{\mu}_{m,n}|m\mu,n\mu\rangle$, where $\mu = H,V$ and $\alpha^{H}_{m,n} = -\alpha^{V}_{m,n} = \alpha_{m,n}/\sqrt{2}$. Note that if $\alpha_{m,n} = \delta_{m,d-n+1}/\sqrt{d}$, for example, we have a maximally entangled state.

The density operator describing the down-converted photons transmitted by the multiple slits is given by $\rho = \alpha^{\mu}_{m,n}\alpha^{\mu'*}_{m',n'}|m\mu,n\mu\rangle\langle m'\mu',n'\mu'|$. The action of a dephasing channel can be represented by a completely positive map with the Kraus representation [34] $\varepsilon(\rho) = p_{hj}K_{hj}\rho K^{\dagger}_{hj}$, where $h,j = 0,\ldots,d$ and K_{hj} are the Kraus operators with $K_{hj} = K_h \otimes K_j$, as well as K_h and K_j acting over the signal and idler subspaces, respectively. Here $\{p_{hj}\}$ are the weighting statistical factors. The dynamics in this process preserves the density operator trace, which means $p_{hj}K^{\dagger}_{hj}K_{hj} = \mathbb{1}\otimes\mathbb{1}$ and $\sum_{h,j} p_{hj} = 1$.

A transmissive spatial light modulator (SLM) is inserted into the path of both the signal and idler beams to apply the SU(d) operations and the dephasing channels. The SLM adds a different phase for each slit mode labeled by m (signal) and n (idler) when we image the slits on the SLM screen. For this end, we use the L_C and L_i lenses to project a magnified image of the multiple slits at the SLM plane (the magnification was necessary to match each slit with a pixel row of the SLM). We split the SLM screen horizontally in two regions (one for each photon) and vertically in d regions (one for each slit mode) such that we can choose different gray scales for these regions in the SLM control software, corresponding to different phase values added to the slit modes. The SLM modulates only the H polarization, which is an important feature for the conditional operation on the superposition between an evolved state H modified by the SLM and an unchanged state V.

We introduce now the Kraus operators that implement the unitary operations leading to the FTP as well as the dephasing noise. The SU(d) operations implemented are represented by diagonal matrices that can be written as $U = e^{i\xi_p}|p\rangle\langle p|$ and $V = e^{i\chi_q}|q\rangle\langle q|$ $(p,q = 1,\ldots,d)$. Here $\xi_p(t)$ and $\chi_q(t)$ are controllable phases, parametrized by t. The evolution under the application of U and V can be described by a map with only one Kraus operator, which can be written as $T = (e^{i\xi_p\delta_{H\alpha}}|p\rangle\langle p|\otimes|\alpha\rangle\langle\alpha|)_s \otimes (e^{i\chi_q\delta_{H\beta}}|q\rangle\langle q|\otimes|\beta\rangle\langle\beta|)_i$. The projectors $|p\rangle\langle p|$ ($|q\rangle\langle q|$) and $|\alpha\rangle\langle\alpha|$ ($|\beta\rangle\langle\beta|$) act over the transverse path subspace and the polarization subspace, respectively, for the signal (idler) photon. The dephasing noise is implemented through a π phase shift randomly added to the photon paths such that its Kraus representation can be written as $D_{hj} = (e^{i\pi\delta_{hp}\delta_{H\alpha}}|p\rangle\langle p|\otimes|\alpha\rangle\langle\alpha|)_s \otimes (e^{i\pi\delta_{jq}\delta_{H\beta}}|q\rangle\langle q|\otimes|\beta\rangle\langle\beta|)_i$. To implement this map along with the map T, we program several masks for the SLM. First, we choose the same set of gray scales (matching the slit modes) specified according to the values of ξ_p and χ_q for all masks. These values are known by the parametrization describing the SU(d) evolution. Then we modify one gray scale of each mask accounting for the addition of a π phase in a certain slit mode, which characterizes the action of a Kraus operator with a certain index h or j $(h,j = 0,\ldots,d)$, except for the mask implementing $D_{00} = \mathbb{1}\otimes\mathbb{1}$ in which no π phase is added to any slit mode.

To guarantee the randomness of the π phase addition, we divide the acquisition time into $(d+1)^2$ intervals. One of them is used for the D_{00} mask, while the others correspond to the $D_{hj\neq 00}$ masks and have the same duration. We then run a film on the SLM screen [35] during the acquisition time with different masks appearing within a certain time interval. Once the photon pair generation is random, one does not know which masks act on each pair, ensuring the desired randomness. Depending on how intense we wish the noise to

be, we can decrease the D_{00} interval duration and increase the time interval of the other masks. For example, if we have two qubits and a 10-s acquisition time, we can make a 100% noise taking 1.25 s for the eight masks corresponding to the $D_{hj\neq 00}$ operators and leaving the D_{00} aside. For a 75% noise we take 0.9375 s to the $D_{hj\neq 00}$ operators and 2.5 s to D_{00}. The 50% noise is achieved taking 0.625 s for each $D_{hj\neq 00}$ and 5 s for D_{00}. Finally, for 0% noise we let D_{00} act over the entire 10-s interval.

The maps are applied to the $|mH, nH\rangle$ terms only. Then, by adding a scanning phase, which is independent of the slit modes, between the $|mH, nH\rangle$ and the $|mV, nV\rangle$ terms, we produce interference patterns for different stages of the evolution and compare their visibilities and phase displacements. From this comparison one can perceive the SU(d) and noise dephasing influences. This scanning phase is added by the phase shifter, whose Kraus representation contains only the operator $S = (\mathbb{1} \otimes \mathbb{1})_s \otimes (e^{-i4\theta\delta_{H\beta}}\mathbb{1} \otimes |\beta\rangle\langle\beta|)_i$.

By composing all the maps in a way similar to that in [31], we get the state $\varepsilon(\rho) = \varepsilon_S \circ \varepsilon_D \circ \varepsilon_T(\rho)$ just before the HWP in front of the detectors:

$$\begin{aligned}\varepsilon(\rho) &= p_{hj} F^{\mu}_{hm,jn} F^{\mu'*}_{hm',jn'} |m\mu, n\mu\rangle\langle m'\mu', n\mu'|,\\ F^{\mu}_{hm,jn} &= \alpha^{\mu}_{m,n} f^{\mu}_{hm,jn},\\ f^{\mu}_{hm,jn} &= (-1)^{(\delta_{hm}+\delta_{jn})\delta_{H\mu}} e^{i(\xi_m+\chi_n-4\theta)\delta_{H\mu}}.\end{aligned} \tag{3}$$

The desired interference between the evolved state terms $|mH, nH\rangle$ and $|mV, nV\rangle$ requires erasure of the polarization information. This task is done by a HWP at 22.5° with the horizontal direction and a PBS placed before the detectors, which erases the polarization information and gives the field operators at the detectors plane as $E^+_1 = \frac{1}{\sqrt{2}}(E^+_{SH} + E^+_{SV})$ and $E^+_2 = \frac{1}{\sqrt{2}}(E^+_{IH} + E^+_{IV})$, where $E^+_{f\mu}$ ($f = S, I$ and $\mu = H, V$) are the positive-frequency components of the field operators before the HWP-PBS set and the indices S and I stand for signal and idler photons, respectively. They can be expanded in terms of the slit mode functions and the annihilation operators that act on the states $|m\mu, n\mu\rangle$, as shown in [22–24,31]. This allows us to calculate the coincidence count $C = \beta\,\mathrm{Tr}\{E^+_2 E^+_1[\varepsilon(\rho)]E^-_1 E^-_2\}$, β being the detection efficiency. In this calculation we must integrate over the detector's transverse position and make use of the orthonormality condition obeyed by the slit mode functions, since all the slit modes are superposed on the same area of each respective detector. Considering an ideal situation where $\beta = 1$, we have as a result

$$\begin{aligned}C &= \tfrac{1}{8}[2 - |\alpha_{m,n}|^2 p_{hj}(f_{hm,jn} + f^*_{hm,jn})]\\ &= \tfrac{1}{4}[1 - |\alpha_{m,n}|^2 p_{hj}(-1)^{(\delta_{hm}+\delta_{jn})}\cos(\xi_m + \chi_n - 4\theta)],\end{aligned} \tag{4}$$

where we make explicit the sum over the polarization index in Eq. (3).

The experiment is performed with the SU(d) parameters shown in Table I, where $\xi_m(t)$ and $\chi_n(t)$ are controlled with a single parameter $t \in [0, 1]$. We generate two-qudit entangled states with dimensions 2, 3, and 4 in the transverse path subspace.

TABLE I. Phase values at different instants t of the SU(d) evolution for two-qubit, two-qutrit, and two-ququart cases.

Principal phases				
t	$\xi_1 = \chi_1$	$\xi_2 = \chi_2$		
0	0	0		
$\frac{1}{2}$	$\pi/4$	$-\pi/4$		
1	$\pi/2$	$-\pi/2$		
t	$\xi_1 = \chi_1$	$\xi_2 = \chi_2$	$\xi_3 = \chi_3$	
0	0	0	0	
$\frac{1}{2}$	$\pi/3$	$-\pi/3$	0	
1	$\pi/3$	$-2\pi/3$	$\pi/3$	
t	$\xi_1 = \chi_1$	$\xi_2 = \chi_2$	$\xi_3 = \chi_3$	$\xi_4 = \chi_4$
0	0	0	0	0
$\frac{1}{2}$	$-\pi/8$	$\pi/8$	$3\pi/8$	$-3\pi/8$
1	$-5\pi/4$	$\pi/4$	$7\pi/4$	$-3\pi/4$

The state prepared corresponds to the one shown in Eq. (2) with $\alpha_{m,n} = \delta_{m,d-n+1}/\sqrt{d}$. This correspond to maximally entangled sates, for which all dynamical phases vanish under SU(d) evolution. Nonmaximally entangled states can experience the fractional topological phase provided α is a full rank matrix; otherwise the cyclic evolution is not restricted to fractional phases. The noise operations are performed by making $p_{hj} = p_h p_j$ and

$$p_h = p_j = \begin{cases} 1-p & \text{if } h, j = 0\\ \frac{p}{d} & \text{if } h, j \neq 0.\end{cases} \tag{5}$$

First, we check the path correlations as well as the polarization entanglement for our state preparation as done in [24]. Then we program the SLM to insert the phases shown in Table I during the whole acquisition time, which correspond to the 0% noise case as discussed before. We measure the coincidence counts while scanning the phase shifter for each one of the three values chosen for the parameter t, ending up with three interference patterns. The results for ququarts ($d = 4$) are shown in Fig. 2(a).

Along with the experimental points we plot the theoretical fit according to

$$C = A[1 + v\cos(4\theta + \delta)]. \tag{6}$$

Such an expression is compatible with Eq. (4) for $v = |p_{hj}\varphi_{hj}|$ and $\delta = \arg\{p_{hj}\varphi_{hj}\}$, where $\varphi_{hj} = |\alpha_{m,n}|^2 e^{i[\pi(\delta_{hm}+\delta_{jn})+\xi_m+\chi_n-4\theta]}$ is the inner product between the evolved and the unchanged states. From the fitting parameters we obtain the FTP experimentally by setting $\gamma_{\mathrm{expt}} = |\delta(t = 1) - \delta(t = 0)|$. The values of v and δ provided by the fitting software for the 0% noise case are shown in the first row of Table II. We expect the value of γ_{expt} to agree with the theoretical prediction $\gamma_{\mathrm{theor}} = 2\pi/d$, which is verified given that $\gamma^{d=2}_{\mathrm{expt}} = 176° \pm 6°$, $\gamma^{d=3}_{\mathrm{expt}} = 125° \pm 7°$, and $\gamma^{d=4}_{\mathrm{expt}} = 89° \pm 7°$ ($\gamma^{d=2}_{\mathrm{expt}}$ and $\gamma^{d=3}_{\mathrm{expt}}$ are obtained from the data in the Appendix). These values agree with the results presented in [24] within the error bars.

Now, to take into account the dephasing noise in the qudits evolution we reprogram the SLM with the films including the random phase π within a certain interval of the acquisition

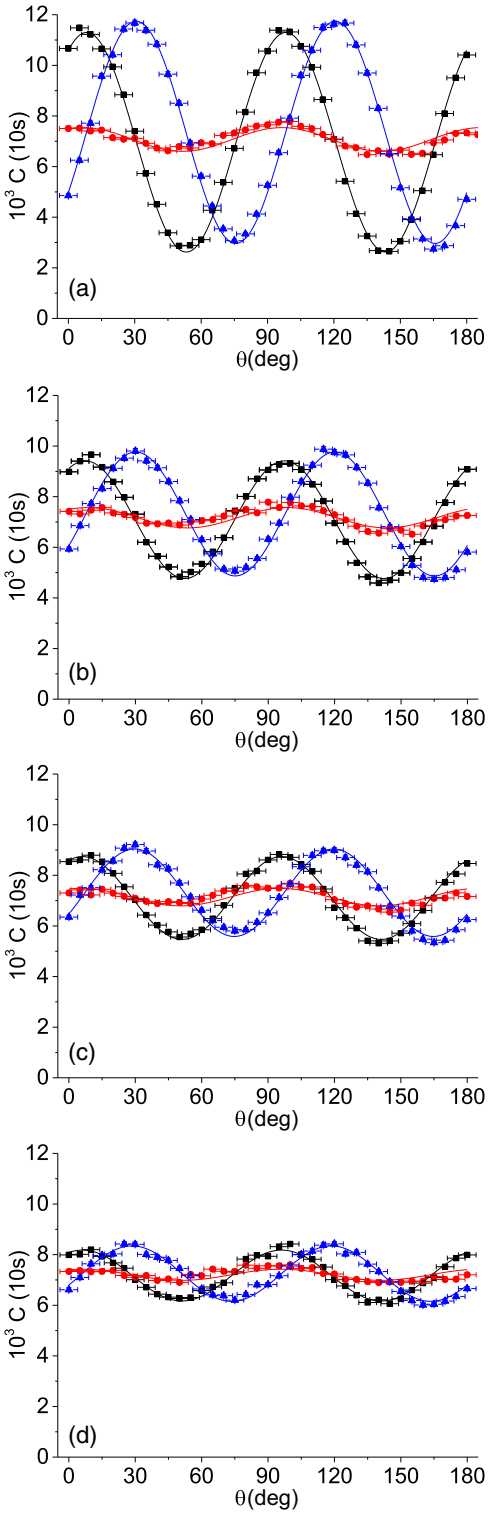

FIG. 2. Interference patterns in the two-photon coincidence counts C for two ququarts. The solid lines are the fitting curves according to Eq. (6). Black squares correspond to $t = 0$, red circles to $t = 0.5$, and blue triangles to $t = 1$. The noise level is (a) 0%, (b) 50%, (c) 75%, and (d) 100%.

time. We choose three different intervals corresponding to noise intensities of 50%, 75%, and 100%, which is equivalent to setting $p = \frac{1}{2}, \frac{3}{4}$, and 1, respectively, in Eq. (5). The results for ququarts are shown in the graphs of Figs. 2(b)–2(d). The corresponding fitting values for v and δ are shown in Table II. The complete results for qubits, qutrits, and ququarts can be seen in the Appendix. The FTP values obtained under noise are summarized in Table III. We clearly see the FTP robustness to the dephasing noise through the preservation of the phase displacement in the interference patterns caused by the SU(d) evolution.

TABLE II. Fitting parameters for ququarts.

Noise	$t = 0$	$t = 0.5$	$t = 1$
0%	$v = 0.623 \pm 0.006$	$v = 0.066 \pm 0.006$	$v = 0.597 \pm 0.006$
0%	$\delta = 33.2 \pm 0.5$	$\delta = 26 \pm 5$	$\delta = 122.7 \pm 0.6$
50%	$v = 0.328 \pm 0.005$	$v = 0.056 \pm 0.006$	$v = 0.335 \pm 0.005$
50%	$\delta = 29.2 \pm 0.9$	$\delta = 34 \pm 6$	$\delta = 120.4 \pm 0.9$
75%	$v = 0.230 \pm 0.004$	$v = 0.048 \pm 0.005$	$v = 0.236 \pm 0.005$
75%	$\delta = 25 \pm 1$	$\delta = 21 \pm 7$	$\delta = 119 \pm 1$
100%	$v = 0.140 \pm 0.004$	$v = 0.030 \pm 0.005$	$v = 0.151 \pm 0.004$
100%	$\delta = 24 \pm 1$	$\delta = 24 \pm 9$	$\delta = 114 \pm 1$

The visibility of the measured interference patterns decreases and increases while the parameter t goes through its interval for a given noise level. The higher the noise level, the lower its maximum value, which occurs for $t = 0$ and 1. To better visualize it, Fig. 3 plots the visibility as a function of the noise level for these two instants and for each measured dimension.

We also plotted the theoretical prediction [31], which led us to make the following normalization of the experimental data for comparison: $v_{\text{norm}}(p) = v(p)/v(0)$, where $v(p)$ is the interference pattern visibility with dephasing weight p.

We see consistent agreement between the experimental points and the theoretical curve. We also note that when applying 100% noise ($p = 1$), the visibilities for qutrits and ququarts exhibit a certain coherence resilience in their interference patterns. There is a distinct behavior for $d = 2$ in comparison with $d > 2$ cases. It has been demonstrated theoretically that qudits are less sensitive to noise with Bell inequality tests and more robust to some eavesdropping attack in quantum cryptography [36–39]. These previous works corroborate our results.

In conclusion, we demonstrated experimentally the robustness of the fractional topological phase to dephasing noise. Two-qudit states are encoded in the transverse linear momentum modes of the entangled photon pairs. Under the action of local SU(d) ⊗ SU(d) operations, they acquire a fractional topological phase measured from two-photon interference patterns. We carried out measurements for the dimensions $d = 2$, 3, and 4 under different noise levels. All measured values agree with the theoretical prediction of $2\pi/d$. For the

TABLE III. Measured topological phases for qubits, qutrits, and ququarts, under different noise levels.

Noise	Qubits	Qutrits	Ququarts
50%	$178^\circ \pm 7^\circ$	$128^\circ \pm 7^\circ$	$91^\circ \pm 7^\circ$
75%	$179^\circ \pm 12^\circ$	$125^\circ \pm 8^\circ$	$94^\circ \pm 7^\circ$
100%		$122^\circ \pm 10^\circ$	$90^\circ \pm 7^\circ$

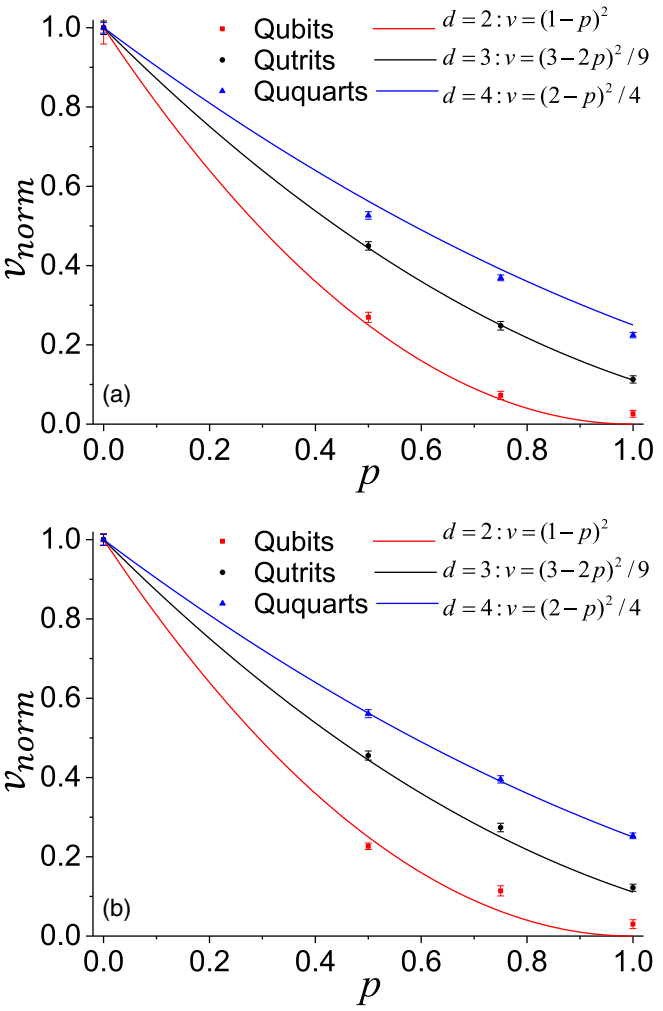

FIG. 3. Normalized experimental visibilities as a function of the noise level: (a) visibility when the SU(d) evolution starts and (b) visibility at the end of the SU(d) evolution. The experimental points for qudits with $d = 2$ (red squares), $d = 3$ (black circles), and $d = 4$ (blue triangles) are plotted along with the theoretical curves [31] (solid lines).

$d = 2$ and 100% noise case, the measured interference patterns confirm the theoretical prediction of complete decoherence. For dimensions larger than $d = 2$, we observed a *coherence resilience*, given the nonzero visibility obtained even for 100% noise level. These results provide strong evidence that the fractional topological phase is a reliable candidate for noise robust quantum processing [40–42].

We are grateful to Raphael Drumond and Leonardo Neves for useful discussions. Funding was provided by Conselho Nacional de Desenvolvimento Científico e Tecnológico, Instituto Nacional de Ciência e Tecnologia de Informação Quântica (INCT-IQ Grant No. 465469/2014-0), Coordenação de Aperfeiçoamento de Pessoal de Nível Superior, Fundação Carlos Chagas Filho de Amparo à Pesquisa do Estado do Rio de Janeiro, and Fundação de Amparo à Pesquisa do Estado de Minas Gerais.

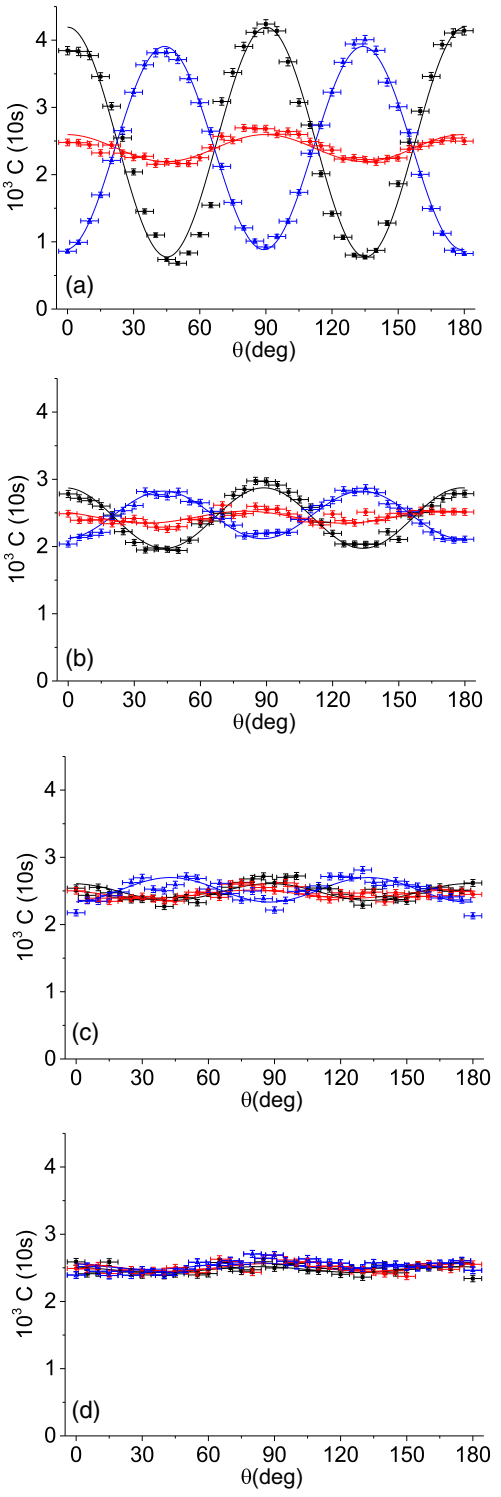

FIG. 4. Interference patterns in the two-photon coincidence counts C for two qubits. The solid lines are the fitting curves according to Eq. (6). Black squares correspond to $t = 0$, red circles to $t = 0.5$, and blue triangles to $t = 1$. The noise level is (a) 0%, (b) 50%, (c) 75%, and (d) 100%.

APPENDIX

The measured interference patterns to observe the fractional topological phase for two qudits with dimensions 2 and 3 are shown in Figs. 4(a) and 5(a). As done in the ququart

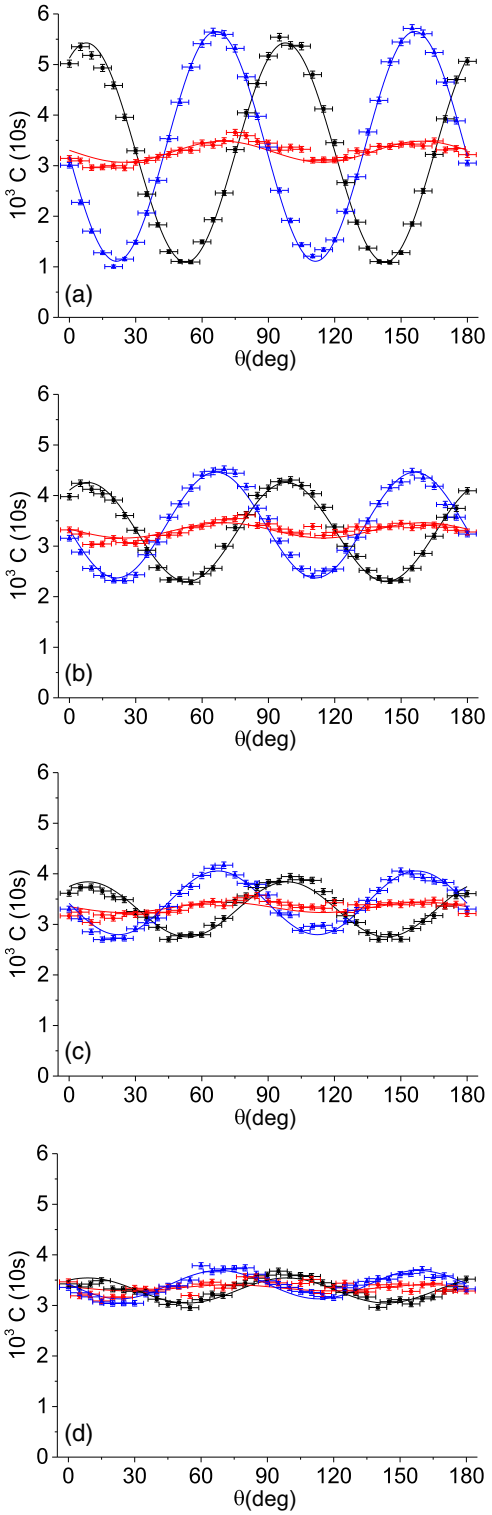

FIG. 5. Interference patterns in the two-photon coincidence counts C for two qutrits. The solid lines are the fitting curves according to Eq. (6). Black squares correspond to $t = 0$, red circles to $t = 0.5$, and blue triangles to $t = 1$. The noise level is (a) 0%, (b) 50%, (c) 75%, and (d) 100%.

TABLE IV. Fitting parameters.

Noise	Fit	Qubits	Qutrits	Ququarts
0%	$A(0)$	2484 ± 40	3258 ± 16	6961 ± 25
0%	$v(0)$	0.69 ± 0.02	0.665 ± 0.008	0.623 ± 0.006
0%	$\delta(0)$	0 ± 2	30.6 ± 0.6	33.2 ± 0.5
0%	$A(1/2)$	2395 ± 12	3275 ± 17	7071 ± 28
0%	$v(1/2)$	0.084 ± 0.007	0.063 ± 0.008	0.066 ± 0.006
0%	$\delta(1/2)$	−1 ± 5	278 ± 7	26 ± 5
0%	$A(1)$	2396 ± 10	3381 ± 14	7352 ± 31
0%	$v(1)$	0.631 ± 0.006	0.672 ± 0.007	0.597 ± 0.006
0%	$\delta(1)$	176.3 ± 0.5	−94.9 ± 0.5	122.7 ± 0.6
50%	$A(0)$	2423 ± 13	3278 ± 13	7090 ± 25
50%	$v(0)$	0.186 ± 0.007	0.299 ± 0.006	0.328 ± 0.005
50%	$\delta(0)$	−5 ± 2	33 ± 1	29.2 ± 0.9
50%	$A(1/2)$	2436 ± 10	3311 ± 15	7168 ± 29
50%	$v(1/2)$	0.037 ± 0.006	0.045 ± 0.007	0.056 ± 0.006
50%	$\delta(1/2)$	−38 ± 9	−80 ± 8	34 ± 6
50%	$A(1)$	2470 ± 9	3416 ± 17	7316 ± 28
50%	$v(1)$	0.143 ± 0.005	0.306 ± 0.007	0.335 ± 0.005
50%	$\delta(1)$	173 ± 2	−95 ± 1	120.4 ± 0.9
75%	$A(0)$	2484 ± 13	3296 ± 16	7103 ± 21
75%	$v(0)$	0.050 ± 0.007	0.165 ± 0.007	0.230 ± 0.004
75%	$\delta(0)$	−8 ± 8	34 ± 2	25 ± 1
75%	$A(1/2)$	2452 ± 11	3336 ± 16	7139 ± 28
75%	$v(1/2)$	0.024 ± 0.006	0.031 ± 0.007	0.048 ± 0.005
75%	$\delta(1/2)$	−40 ± 15	−81 ± 13	21 ± 7
75%	$A(1)$	2517 ± 15	3426 ± 16	7311 ± 27
75%	$v(1)$	0.072 ± 0.008	0.184 ± 0.007	0.236 ± 0.005
75%	$\delta(1)$	171 ± 7	−91 ± 2	119 ± 1
100%	$A(0)$	2474 ± 10	3295 ± 14	7175 ± 19
100%	$v(0)$	0.018 ± 0.006	0.075 ± 0.006	0.140 ± 0.004
100%	$\delta(0)$	−28 ± 19	35 ± 5	24 ± 1
100%	$A(1/2)$	2506 ± 10	3348 ± 18	7204 ± 26
100%	$v(1/2)$	0.023 ± 0.006	0.018 ± 0.007	0.030 ± 0.005
100%	$\delta(1/2)$	−12 ± 14	−67 ± 23	24 ± 9
100%	$A(1)$	2528 ± 12	3410 ± 14	7249 ± 22
100%	$v(1)$	0.019 ± 0.007	0.082 ± 0.006	0.151 ± 0.004
100%	$\delta(1)$	−47 ± 20	−87 ± 4	114 ± 1

case, we plotted the theoretical fit according to Eq. (6). The values provided by the fitting software are shown in Table IV (the data for ququarts are show again, including the amplitude parameter). The measured interference patterns to observe the fractional topological phase for the two qudits under dephasing noise are also presented, shown in the graphs of Figs. 4(b)–4(d) and 5(b)–5(d). We see that the FTP is preserved in all cases, except for $d = 2$ at 100% noise. This agrees with the theoretical prediction of zero visibility for 100% noise in two qubits as shown in [31]. The effect of the noise is to diminish the visibility for any instant t, but we still see the same behavior of the visibility dropping to near 0 for $t = 0.5$ and approximately recovering the value of $t = 0$ when $t = 1$.

[1] S. Pancharatnam, Generalized theory of interference, and its applications, Proc. Indian Acad. Sci. A **44**, 247 (1956).

[2] M. Berry, Quantal phase factors accompanying adiabatic changes, Proc. R. Soc. London Ser. A **392**, 45 (1984).

[3] Y. Aharonov and J. Anandan, Phase Change During a Cyclic Quantum Evolution, Phys. Rev. Lett. **58**, 1593 (1987).

[4] A. Carollo, I. Fuentes-Guridi, M. F. Santos, and V. Vedral, Geometric Phase in Open Systems, Phys. Rev. Lett. **90**, 160402 (2003).

[5] A. Tomita and R. Y. Chiao, Observation of Berry's Topological Phase by Use of an Optical Fiber, Phys. Rev. Lett. **57**, 937 (1986).

[6] T. Bitter and D. Dubbers, Manifestation of Berry's Topological Phase in Neutron Spin Rotation, Phys. Rev. Lett. **59**, 251 (1987).

[7] D. J. Richardson, A. I. Kilvington, K. Green, and S. K. Lamoreaux, Demonstration of Berry's Phase Using Stored Ultracold Neutrons, Phys. Rev. Lett. **61**, 2030 (1988).

[8] P. G. Kwiat and R. Y. Chiao, Observation of a Nonclassical Berry's Phase for the Photon, Phys. Rev. Lett. **66**, 588 (1991).

[9] E. Sjöqvist, Geometric phase for entangled spin pairs, Phys. Rev. A **62**, 022109 (2000).

[10] B. Hessmo and E. Sjöqvist, Quantal phase for nonmaximally entangled photons, Phys. Rev. A **62**, 062301 (2000).

[11] P. Milman and R. Mosseri, Topological Phase for Entangled Two-Qubit States, Phys. Rev. Lett. **90**, 230403 (2003).

[12] P. Milman, Phase dynamics of entangled qubits, Phys. Rev. A **73**, 062118 (2006).

[13] D. M. Tong, E. Sjöqvist, L. C. Kwek, and C. H. Oh, Kinematic Approach to the Mixed State Geometric Phase in Nonunitary Evolution, Phys. Rev. Lett. **93**, 080405 (2004).

[14] J. Du, P. Zou, M. Shi, L. C. Kwek, J.-W. Pan, C. H. Oh, A. Ekert, D. K. L. Oi, and M. Ericsson, Observation of Geometric Phases for Mixed States using NMR Interferometry, Phys. Rev. Lett. **91**, 100403 (2003).

[15] E. Sjöqvist, A. K. Pati, A. Ekert, J. S. Anandan, M. Ericsson, D. K. L. Oi, and V. Vedral, Geometric Phases for Mixed States in Interferometry, Phys. Rev. Lett. **85**, 2845 (2000).

[16] C. E. R. Souza, J. A. O. Huguenin, P. Milman, and A. Z. Khoury, Topological Phase for Spin-Orbit Transformations on a Laser Beam, Phys. Rev. Lett. **99**, 160401 (2007).

[17] J. Du, J. Zhu, M. Shi, X. Peng, and D. Suter, Experimental observation of a topological phase in the maximally entangled state of a pair of qubits, Phys. Rev. A **76**, 042121 (2007).

[18] L. E. Oxman and A. Z. Khoury, Fractional Topological Phase for Entangled Qudits, Phys. Rev. Lett. **106**, 240503 (2011).

[19] M. Johansson, M. Ericsson, K. Singh, E. Sjöqvist, and M. S. Williamson, Topological phases and multiqubit entanglement, Phys. Rev. A **85**, 032112 (2012).

[20] M. Johansson, A. Z. Khoury, K. Singh, and E. Sjöqvist, Three-qubit topological phase on entangled photon pairs, Phys. Rev. A **87**, 042112 (2013).

[21] J. C. Loredo, M. A. Broome, D. H. Smith, and A. G. White, Observation of Entanglement-Dependent Two-Particle Holonomic Phase, Phys. Rev. Lett. **112**, 143603 (2014).

[22] A. Z. Khoury, L. E. Oxman, B. Marques, A. Matoso, and S. Pádua, Fractional topological phase on spatially encoded photonic qudits, Phys. Rev. A **87**, 042113 (2013).

[23] A. A. Matoso, X. Sánchez-Lozano, W. M. Pimenta, P. Machado, B. Marques, F. Sciarrino, L. E. Oxman, A. Z. Khoury, and S. Pádua, Experimental observation of fractional topological phases with photonic qudits, Phys. Rev. A **94**, 052305 (2016).

[24] A. A. Matoso, R. A. Ribeiro, L. E. Oxman, A. Z. Khoury, and S. Pádua, Fractional topological phase measurement with a hyperentangled photon source, Sci. Rep. **9**, 577 (2019).

[25] F. C. Lombardo and P. I. Villar, Geometric phases in open systems: A model to study how they are corrected by decoherence, Phys. Rev. A **74**, 042311 (2006).

[26] F. C. Lombardo and P. I. Villar, Environmentally induced corrections to the geometric phase in a two-level system, Int. J. Quantum Inf. **06**, 707 (2008).

[27] P. I. Villar, Spin bath interaction effects on the geometric phase, Phys. Lett. A **373**, 206 (2009).

[28] F. C. Lombardo and P. I. Villar, Environmentally induced effects on a bipartite two-level system: Geometric phase and entanglement properties, Phys. Rev. A **81**, 022115 (2010).

[29] P. I. Villar and F. C. Lombardo, Geometric phases in the presence of a composite environment, Phys. Rev. A **83**, 052121 (2011).

[30] L. E. Oxman, A. Z. Khoury, F. C. Lombardo, and P. I. Villar, Two-qudit geometric phase evolution under dephasing, Ann. Phys. (NY) **390**, 159 (2018).

[31] R. A. Ribeiro, A. A. Matoso, L. E. Oxman, A. Z. Khoury, and S. Pádua, Robustness of the fractional topological phase to dephasing, Phys. Rev. A **99**, 042101 (2019).

[32] P. G. Kwiat, E. Waks, A. G. White, I. Appelbaum, and P. H. Eberhard, Ultrabright source of polarization-entangled photons, Phys. Rev. A **60**, R773 (1999).

[33] L. Neves, G. Lima, J. G. Aguirre Gómez, C. H. Monken, C. Saavedra, and S. Pádua, Generation of Entangled States of Qudits using Twin Photons, Phys. Rev. Lett. **94**, 100501 (2005).

[34] M. A. Nielsen and I. L. Chuang, *Quantum Computation and Quantum Information*, 10th ed. (Cambridge University Press, Cambridge, 2010).

[35] B. Marques, A. Matoso, W. Pimenta, A. J. Gutiérrez-Esparza, M. Santos, and S. Pádua, Experimental simulation of decoherence in photonics qudits, Sci. Rep. **5**, 16049 (2015).

[36] D. Kaszlikowski, P. Gnaciński, M. Żukowski, W. Miklaszewski, and A. Zeilinger, Violations of Local Realism by Two Entangled N-Dimensional Systems Are Stronger than for Two Qubits, Phys. Rev. Lett. **85**, 4418 (2000).

[37] H. Bechmann-Pasquinucci and A. Peres, Quantum Cryptography with 3-State Systems, Phys. Rev. Lett. **85**, 3313 (2000).

[38] D. B. C. Bruß and C. Macchiavello, Optimal Eavesdropping in Cryptography with Three-Dimensional Quantum States, Phys. Rev. Lett. **88**, 127901 (2002).

[39] N. J. Cerf, M. Bourennane, A. Karlsson, and N. Gisin, Security of Quantum Key Distribution Using d-Level Systems, Phys. Rev. Lett. **88**, 127902 (2002).

[40] J. A. Jones, V. Vedral, A. Ekert, and G. Castagnoli, Geometric quantum computation using nuclear magnetic resonance, Nature (London) **403**, 869 (2000).

[41] L.-M. Duan, J. I. Cirac, and P. Zoller, Geometric manipulation of trapped ions for quantum computation, Science **292**, 1695 (2001).

[42] A. Kitaev, Fault-tolerant quantum computation by anyons, Ann. Phys. (NY) **303**, 2 (2003).